Journal of The
Electrochemical Society

Electrochemical Ammonia Synthesis in a Proton-Conducting Ceramic Cell: A Parameter Study of an Iron-Based Electrode

To cite this article: Philipp Blanck *et al* 2025 *J. Electrochem. Soc.* **172** 084507

Journal of The Electrochemical Society, 2025 **172** 084507

Electrochemical Ammonia Synthesis in a Proton-Conducting Ceramic Cell: A Parameter Study of an Iron-Based Electrode

Philipp Blanck,[1,2] Etienne P. Martin,[1] Daniel Schmider,[2] Robert J. Kee,[3,*] Julian Dailly,[2,z] and Olaf Deutschmann[1]

[1]*Technology (KIT), Institute for Chemical Technology and Polymer Chemistry (ITCP), Karlsruhe 76131, Germany*
[2]*European Institute for Energy Research (EIfER), Karlsruhe 76131, Germany*
[3]*Colorado School of Mines (CSM), Department of Mechanical Engineering, Golden 80401, United States of America*

Proton-conducting ceramic cells with a Ni-$BaCe_{0.8}Zr_{0.1}Y_{0.1}O_{3-\delta}$ ‖ $BaCe_{0.7}Zr_{0.2}Y_{0.1}O_{3-\delta}$ ‖ Fe/$BaCe_{0.7}Zr_{0.2}Y_{0.1}O_{3-\delta}$ -backbone structure were studied in a dual-chamber setup to evaluate the effects of temperature, gas flow, voltage, and electrolyte thickness on electrochemical ammonia synthesis. Three gas feed configurations were tested to differentiate surface reaction mechanisms. Thermodynamic calculations were conducted to evaluate the experimental results in the context of equilibrium limitations. The results showed that proton transport through the electrolyte plays a minor role in the formation of ammonia, while production rates correlated more strongly with applied voltage than with current density. Ammonia synthesis appeared significantly limited by thermodynamics, making an increased hydrogen partial pressure at the cathode essential. A feed configuration supplying only nitrogen to the cathode was ineffective, whereas introducing hydrogen increased the ammonia formation rate from 1.42×10^{-10} mol cm^{-2} s^{-1} to 3.23×10^{-9} mol cm^{-2} s^{-1} at −1.4 V and 500 °C. When proton conduction was suppressed under the same conditions, the rate further increased to 4.32×10^{-9} mol cm^{-2} s^{-1}. Varying the cathodic gas flow rate across the 12.57 cm^2 active area from 8 NL h^{-1} to 20 NL h^{-1}, the ammonia formation rate improved by a factor of 3.1 at −1 V, at both 500 °C and 600 °C.
 [DOI: 10.1149/1945-7111/adfc9e]

Manuscript submitted June 12, 2025; revised manuscript received July 28, 2025. Published August 29, 2025.

Supplementary material for this article is available online

Ammonia (NH_3) is a cornerstone of the chemical industry, essential for fertilizer production and various industrial applications. Its conventional synthesis via the Haber–Bosch process is highly energy-intensive, operating under pressures of 20 MPa to 40 MPa and temperatures between 400 °C and 500 °C. In 2020, NH_3 production exceeded 185 metric million tons, with demand expected to rise by 37% by 2050.[1] According to the International Energy Agency (IEA), NH_3 synthesis accounts for around 2% of global final energy consumption and 1.3% of anthropogenic CO_2 emissions, making it the most energy-intensive chemical process worldwide.[2] The current reliance on fossil fuel-derived hydrogen (H_2) further exacerbates its carbon footprint, with each ton of NH_3 produced generating an average of 2.4 tons of CO_2.[2]

To address the challenges associated with sustainable NH_3 synthesis, recent advances have focused on proton-conducting ceramic cells (PCCs).[3–5] These systems operate under milder conditions and represent a promising alternative to the conventional Haber-Bosch process. Figure 1 shows a schematic representation of the reactions occurring during electrochemical NH_3 synthesis on a PCC.

At the anode, a hydrogen carrier, such as water (H_2O) or in this study H_2 itself, undergoes oxidation, releasing protons (OH_O) that migrate in the direction of the applied current. During NH_3 synthesis at the cathode, protons may react either with dissociated nitrogen (N_2) at the catalyst surface to form NH_3 (pathway a) or participate in the H_2 evolution reaction (HER) to form molecular H_2 (pathway b). In addition, gas-phase as well as thermocatalytic and electrocatalytic reactions (pathway c) that do not involve protons may also contribute to the overall NH_3 formation.

In this context, electrochemical promotion of catalysis (EPOC) has attracted attention. EPOC, also known as non-Faradaic electrochemical modification of catalytic activity (NEMCA), refers to the reversible enhancement of catalytic reaction rates induced by an electric field. This effect takes place on a catalyst film, or a supported catalyst dispersed on an ionic conductive solid electrolyte. The catalytic activity is modified by applying an electric potential between the catalyst and a secondary conductive layer on the opposite side of the electrolyte.

The EPOC effect was first discovered in 1981 by Michael Stoukides and Costas Vayenas and is related to the electrochemical supply of ionic species to the catalyst surface, which, in turn, induce changes in the electronic and chemisorptive properties of the catalyst.[6,7] The induced change in catalytic rate, $\Delta r = r - r_0$, upon catalyst polarization (r is the catalytic reaction rate under closed-circuit conditions, and r_0 is the open-circuit catalytic rate), exceeds the electrocatalytic rate predicted by Faraday's law, which depends on the rate of ion transport through the electrolyte.[8] This phenomenon is captured by the enhancement factor of Faradaic efficiency, Λ (1), which is defined as:

$$\Lambda = \frac{\Delta r n F}{i} \quad [1]$$

where i is the the current, n the number of electrons (with $n = 3$ for NH_3), and F denotes Faraday's constant. Since $i/n F$ denotes the theoretical production rate at 100% Faraday efficiency, a value of Λ greater than 1 is indicative of changes in the catalytic properties of the electrode that go beyond simple charge transfer.[5,9] Additionally, the rate enhancement ratio, ρ (2), given by:

$$\rho = \frac{r}{r_0} = \frac{r_0 + \Delta r}{r_0} \quad [2]$$

represents the ratio of catalytic rates in the presence and absence of polarization. In the case of electrochemical NH_3 synthesis, several studies report Λ values consistently below one, indicating the absence of a significant EPOC effect under their respective conditions (see Table I). This limited EPOC effect, as previously also reported by Garagounis et al., is attributed to the inherent thermodynamic constraints of the ammonia synthesis reaction.[10] In terms to the rate enhancement ratio, typical ρ values ranging from 2 to 10 have been reported, without a clear correlation to the applied electric field strength.[11] A maximum ρ value of 220 was observed by Li et al., using pure iron as the catalyst at a testing temperature of 550 °C.[12] An overview of reported EPOC values from various papers

*Electrochemical Society Member.
[z]E-mail: Julian.Dailly@eifer.org

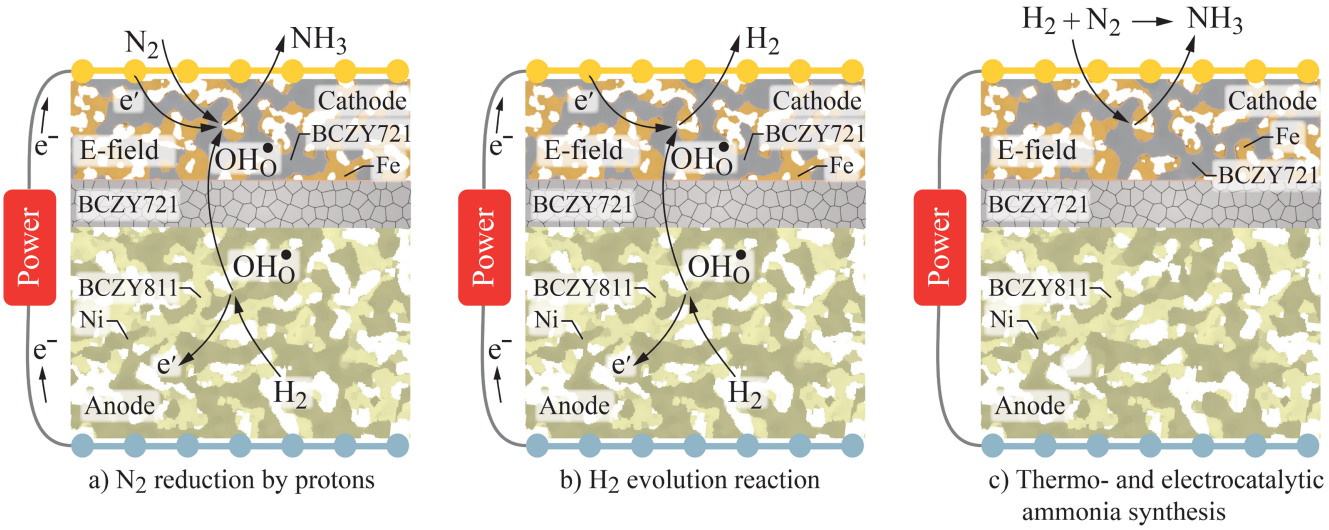

Figure 1. Schematic representation of reactions occurring at a proton-conducting ceramic cell that either contribute to NH_3 synthesis or compete with it. The reactions take place simultaneously.

Table I. Reported and calculated Λ and ρ values from papers including this study using a barium-based electrolyte and a gas mixture of H_2 and N_2 at the cathode.

Year	Λ	ρ	References
2015	0.07[a)]	1.4	13
2016	0.04[a)]	2.4	14
2017	0.003[a)]	20	15
2021	0.15[a)]	220	12
2023	0.06[a)]	10	16
2025	0.012	21	this study

a) Calculated based on reported data.

using barium-based electrolytes is provided in Table I. All the cited publications employ a mixture of H_2 and N_2 at the cathode, as the electrochemical NH_3 synthesis is enhanced by the simultaneous supply of both N_2 and H_2, rather than N_2 alone.

For NH_3 synthesis, EPOC has been observed to be weak, constrained by the equilibrium-limited nature of the reaction at elevated temperatures and the competing HER, resulting in electrochemical Faradaic efficiencies towards NH_3, FE_{NH_3} ($FE_{NH_3} = \Lambda \times 100$) mostly below 10%.[17] Additionally, increasing the applied current enhances the reaction rate up to a point, after which the rate either plateaus or declines.[18,19] This decrease has been attributed to the "poisoning" of the cathode by hydrogen, which inhibits N_2 chemisorption due to the high rate of electrochemically supplied protons.[18,20]

Future advancements in electrochemical NH_3 synthesis will rely on the development of highly selective catalysts to suppress the HER and the optimization of operating parameters with respect to thermodynamic and kinetic considerations. The latter will be the primary focus of this work. This study also investigates the question of whether EPOC plays any role in electrochemical ammonia synthesis.

To place our experimental investigations in context, Table II lists results from other studies also utilizing a dual-chamber setup and supplying a mixture of H_2:N_2 to the cathode. However, data on this configuration remain limited in literature so far.

Experimental

***Powders.*—**All materials used this study are commercially sourced. Anode and electrolyte layers were prepared using $BaCe_{0.8}Zr_{0.1}Y_{0.1}O_{3-\delta}$ (BCZY811) and $BaCe_{0.7}Zr_{0.2}Y_{0.1}O_{3-\delta}$ (BCZY721) (CerPoTech AS), NiO (JT Baker®) and ZnO (Sigma Aldrich). The cathode consisted of BCZY721 (CerPoTech AS) and α-Fe_2O_3 (<5 μm, 96%, Merck). TIMREX SFG75 Graphite (TIMCAL) was used as a pore former.

***Cell fabrication*.— Anode.—**The anode support was prepared via tape casting using a slurry composed of NiO:BCZY811 in a weight ratio of 1.5:1, graphite (pore former), Nuosperse (dispersant), and butanone/ethanol (solvents). The mixture was homogenized with a Turbula® T2F mixer (WAB) for 24 h, followed by the addition of polyvinyl butyral (binder) and PEG/TEG-EH (plasticizers, Eastman), then milled for another 3 h. After resting for 24 h, the slurry was degassed under vacuum for 10 min. It was cast using a ZAA 2300 film applicator (Zehntner GmbH) onto a polymer sheet covered glass plate and dried at room temperature for 24 h, yielding tapes of 500 μm thickness and a surface area of about 700 cm^2. Circular samples (∅ 77 mm) were then cut for further processing.

Electrolyte.—BCZY721 was blended with a carrier mixture (α-terpineol and ethyl cellulose) and 0.5 wt% ZnO (sintering aid), then ground in an automatic mortar (Retsch RM200) for 20 min and further refined using a roller mill. The resulting electrolyte ink was screen-printed onto the green anode tape cutouts using an EKRA E2 screen-printer. For increased electrolyte thicknesses, multiple screen-printing steps were performed with intermediate drying. After drying at room temperature for 1 h, the half-cells were co-sintered at 1400 °C for 8 h, with intermediate dwell steps at 250 °C (solvent evaporation) and 550 °C (graphite burnout of the support electrode).

Cathode.—The cathode was applied via screen-printing in two steps. First, a porous BCZY721 backbone mixture (BCZY721: graphite, weight ratio 1.5:1) dispersed in a carrier mixture (α-terpineol and ethyl cellulose, 45 wt% solids) was printed onto the sintered half-cell, dried in ambient air until matte, and sintered at 1350 °C for 1 h with heating and cooling ramps of 3 K min^{-1}. The obtained porous BCZY721 structure serves as a scaffold for catalyst deposition. Subsequently, a low-viscosity Fe_2O_3 ink (Fe_2O_3 and the same carrier mixture, 45 wt% solids) was "screen-pressed," i.e. using screen-printing to impress the ink into the previously sintered backbone. The cathode was finally calcined at 850 °C for 1 h with 3 K min^{-1} ramps, resulting in a homogeneous distribution of the iron catalyst within the backbone without any detectable interaction with the backbone material.[23] The final cell had a diameter of 52 mm (21.24 cm^2 total area), with an active cathode area of 12.57 cm^2 (40 mm diameter).

Table II. Studies utilizing a dual-chamber setup with mixed N_2 and H_2 supplied to the cathode. Only the peak NH_3 production rates achieved under specific temperature and configuration conditions are displayed. Unless otherwise specified, all results pertain to planar cells.

Year	Anode	Electrolyte	Cathode	Active area [cm^2]	T [°C]	U [V]	r_{NH_3} [10^{-9} mol cm^{-2} s^{-1}]	H_2:N_2	V [NL h^{-1}]	References
2007	Ag	SZY	Fe	2	500	−2	0.11	4:62[a)]	—	21
2016	Cu	BZCY721	Ni-BZCY721	4[b)]	620	2.4	4.1	1:1	9	14
2021	Pt	BCY10	K, Al-Fe-BCY10	0.39	650	−1.5	0.67	15:85	—	15
2021	Pt	BCY10	Fe-BCY10	1	600	−0.7	0.42	1:9	—	12
2021	Pt	BCY10	W-Fe-BCY10	1	550	−1.2	0.57	1:9	—	12
2021	Pt	BCY10	Fe	1	550	−1.2	1.3	1:9	2.4	12
2021	Pt	BCY10	Fe	1	550	−1.2	14	1:1	2.4	12
2024	BCFZY-BCY10	BCY10	Fe	1	600	−1	7.2	1:1	—	22
2025	Ni-BCZY811	BCZY721	Fe/BCZY721-backbone	12.57	500	−1.4	4.32	1:1	12	this study

SZY: $SrZr_{0.95}Y_{0.05}O_{3-a}$, BZCY721: $BaZr_{0.7}Ce_{0.2}Y_{0.1}O_{2.9}$, BCY10: $BaCe_{0.9}Y_{0.1}O_3$, BCFZY: $BaCo_{0.4}Fe_{0.4}Zr_{0.1}Y_{0.1}O_{3-\delta}$, BCZY811: $BaCe_{0.8}Zr_{0.1}Y_{0.1}O_{3-\delta}$, BCZY721: $BaCe_{0.7}Zr_{0.2}Y_{0.1}O_{3-\delta}$. a) Diluted in He. b) Tubular cell.

Electrochemical characterization.—For electrochemical characterization, the PCCs are tested in a double-flange test rig with an aluminum oxide lining. Electrical contact to the NiO-BCZY811 electrode is established using nickel and Inconel 600 wires (∅ 0.5 mm), which are connected to a nickel foam disk (∅ 50 mm). Similarly, a gold grid (∅ 40 mm) with gold wires (∅ 0.5 mm) establishes electrical contact with the iron-containing electrode. A schematic of the assembled cell is presented in Fig. 2.

Ceramabond 552 A2 (T-E-Klebetechnik) is used as sealing, applied in thin layers and dried at room temperature. The mounted cell is subsequently heated at a rate of 1 K min^{-1}, with 2 NL h^{-1} N_2 supplied to both electrodes. Dwell times of 2 h at 100 °C, 260 °C and 650 °C are implemented to cure the seal during start-up. Gas tightness was verified by measuring the downstream volume flow. The cell is gradually reduced at 600 °C by incrementally increasing the H_2 supply to both electrodes until a desired H_2 partial pressure is reached and the cell voltage stabilizes. Once stabilization is achieved, the system is brought to the target temperature for electrochemical characterization and quantitative NH_3 measurements.

The mass of catalyst was estimated from the weight difference before ink application and after sintering, assuming complete reduction of Fe_2O_3 based on its stoichiometry.

Electrochemical Impedance Spectroscopy (EIS) was conducted using a Zahner Zennium (Zahner) instrument over a frequency range of 100 mHz to 100 kHz, with an AC amplitude of 15 mV, measured at OCV (open-circuit voltage).

NH_3 formation was analyzed using a high-performance ion-selective electrode (Orion™, Thermo Scientific™ 9512HPBNWP). For each parameter variation, following a stabilization period of at least 15 min, the outlet gas was directed through a 0.01 M H_2SO_4 solution for 20 min to capture the NH_3. Background measurements were performed between 400 °C to 600 °C at a flow rate of 20 NL h^{-1} using a blank cell without any catalyst applied. Two gas configurations were tested, including the following anode/cathode combinations: H_2/H_2:N_2 (1:1) and H_2/N_2 (see Fig. S1). In addition, pure N_2 was supplied to both electrodes to assess background NH_3 levels, which resulted in formation rates below the detection limit of the ISE.

Results and Discussion

Thermodynamics.—To gain deeper insights for the optimized parameter selection for electrochemical NH_3 synthesis, thermodynamic simulations were performed using the DETCHEM software package. Specifically, the DETCHEM^{EQUIL} code was utilized for thermodynamic calculations displayed in Fig. S2a in Supplementary material.[24]

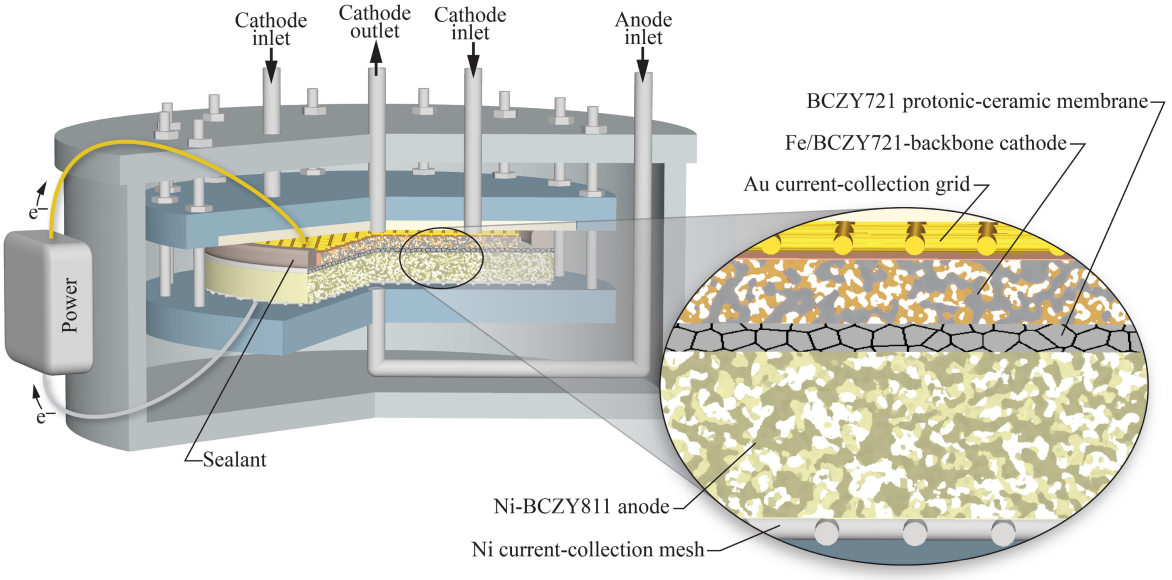

Figure 2. Schematic illustration of the double-flange setup with the cell mounted between the two flanges.

Table III. Tested configurations and the gases supplied to the respective electrodes.

Configuration	Anode [NL h^{-1}]	Cathode [NL h^{-1}]
"classic"	6 H_2 + 6 N_2	6 N_2 + 6 Ar
"mixed"	6 H_2 + 6 N_2	6 H_2 + 6 N_2
"blocked"	6 Ar + 6 N_2	6 H_2 + 6 N_2

The simulations were conducted at atmospheric pressure to align with the available test bench conditions.

The simulations show that, thermodynamically, lower temperatures significantly shift the NH_3 equilibrium toward higher yields for all H_2:N_2 ratios and a stoichiometric H_2:N_2 ratio of 3:1 is preferred for optimal NH_3 formation. However, PCCs face operational limitations at lower temperatures, as proton conductivity decreases sharply below 400 °C. From a thermodynamic perspective, operating PCCs between 400 °C and 500 °C appears to be advantageous, while from a kinetic standpoint, 500 °C may offer a feasible compromise.

In this context, the volumetric flow rate normalized to the cell surface area must be considered, as an increase in this parameter leads to a proportional enhancement in ammonia formation from a thermodynamic perspective (see Fig. S2b).

From a kinetic standpoint, lower normalized volumetric flow rates correspond to longer residence times of reactants at the cathode under operating conditions, which tends to bring the NH_3 concentration closer to equilibrium. Conversely, higher normalized volumetric flow rates reduce the residence time, causing the NH_3 concentration to remain below the equilibrium value.

Reaching the targets established by the DOE (United States Department of Energy) for the commercialization of NH_3 production employing PCCS necessitates achieving a r_{NH_3} of around 10^{-6} mol cm^{-2} s^{-1}, a current density j exceeding 300 mA cm^{-2}, and a Faraday efficiency to ammonia η_{NH_3} of 90%.[25] In their technoeconomic analysis of PCCs for NH_3 synthesis, Moranti et al. propose a target η_{NH_3} in the range of 10^{-7} mol cm^{-2} s^{-1} to 10^{-8} mol cm^{-2} s^{-1} to achieve economic sustainability.[26]

Operating the cell at 500 °C at thermodynamic equilibrium with a H_2:N_2 ratio of 1:1 would require a volumetric flow rate of 23 NL h^{-1} cm^{-2} to achieve the target r_{NH_3} of 10^{-7} mol cm^{-2} s^{-1}. When the temperature is reduced to 400 °C while maintaining the same gas composition and equilibrium conditions, the required volumetric flow rate decreases to 6 NL h^{-1} cm^{-2}. Assuming a more ambitious target for r_{NH_3} of 10^{-6} mol cm^{-2} s^{-1}, the previously stated volumetric flow rates per cell area should be multiplied by a factor of ten.

Mechanistic investigations.—To differentiate the various effects and mechanisms contributing to the electrocatalytic formation of NH_3, three gas configurations were examined. For clarity, these configurations are summarized in Table III. To maintain simplicity, the three gas configurations are referenced throughout the text using the labels provided in the table's first column.

The "classic" configuration, with H_2 and N_2 (1:1) at the anode and N_2 and Ar (1:1) at the cathode, refers to a setup in which NH_3 formation occurs via direct proton transport across the membrane, enabling surface reactions that drive the nitrogen reduction reaction (NRR). Another possible pathway is that protons first undergo HER, generating molecular H_2, which can then react with N_2 either on the catalytic surface or in the gas phase.

In the "mixed" configuration, with H_2 and N_2 (1:1) at the anode and at the cathode, NH_3 formation is assumed to occur via surface protons at the triple-phase boundary, catalytic surface reactions of the involved species, and gas-phase reactions. Previous studies have demonstrated that introducing H_2 to the cathode enhances NH_3 formation, with an H_2:N_2 ratio of 1:1 yielding the highest ammonia formation rates.[12,14]

By varying the H_2:N_2 ratio between 1:1 and 2:1, a slight peak was observed at 500 °C and −1 V at a ratio of 1.2:1 (See Fig. S3). But for easier process control and comparability, the ratio is kept at 1:1 in the following experiments.

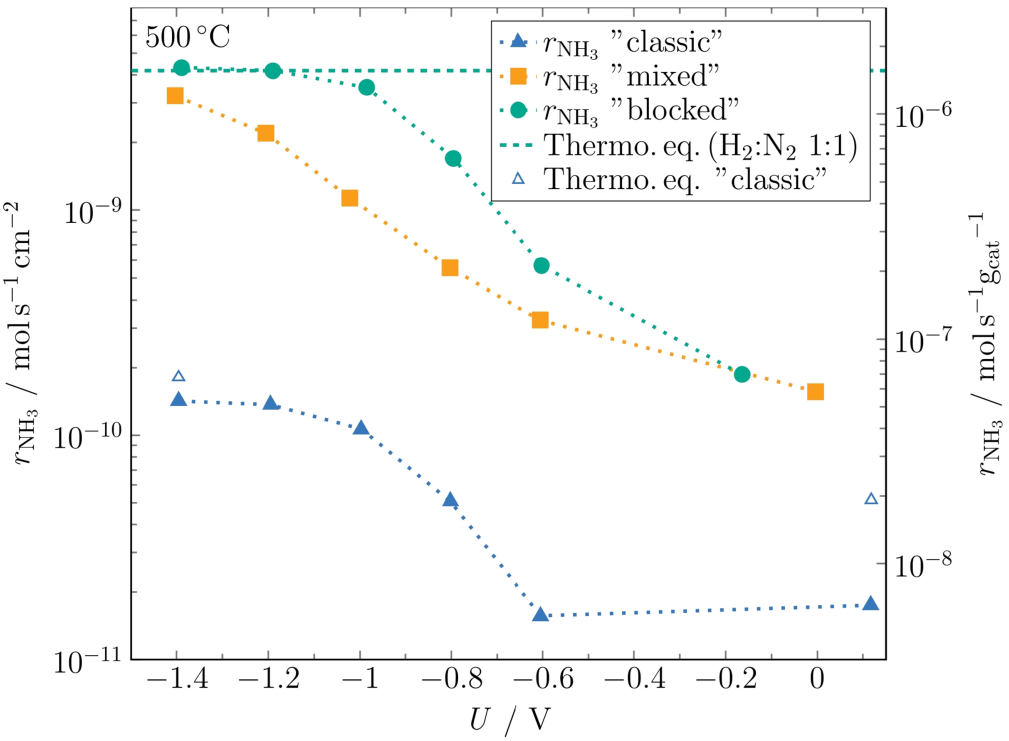

Figure 3. NH_3 formation r_{NH_3} as a function of cell voltage for the three gas configurations from Table III, conducted at 500 °C with a constant volume flow of 12 NL h^{-1}. The thermodynamic equilibrium (green, dashed) is calculated for an active area of 12.57 cm^2, 12 NL h^{-1} and a temperature of 500 °C at OCV. Blue open triangles display the thermodynamic equilibrium for H_2 concentrations measured at the cathode in the "classic" configuration at OCV and −1.4 V.

In the configuration "blocked", with Ar and N_2 (1:1) at the anode and N_2 and H_2 (1:1) at the cathode, proton conduction through the electrolyte is deliberately inhibited by supplying inert gases to the anode, thereby excluding the influence of the pumped protons. This approach enables the isolated assessment of the effect of the applied electrical potential in the absence of ionic flux from the electrolyte, which would otherwise contribute to NH_3 synthesis. To the best of our knowledge, this specific configuration has not been previously described in the literature and cannot be associated directly with EPOC, as the electric field is decoupled from the sustained transport of ionic species.

Thus, it was anticipated that configuration "blocked" would yield lower r_{NH_3} compared to configuration "mixed" since the supply of protons through the electrolyte to the triple phase boundaries of the cathode is suppressed, eliminating one of the possible NH_3 formation pathways.

Figure 3 illustrates the r_{NH_3} normalized to the active area (left) and catalyst loading (right) for the three gas configurations outlined in Table III. The formation rates are plotted as a function of the cell voltage at each point. The measured OCV (open-circuit voltage) for configuration "mixed" is −0.003 V, for "classic" 0.117 V and −0.164 V for "blocked," caused by the different gas compositions at the electrodes. The iron catalyst loading on the 12.57 cm^2 electrode is 2.7 mg_{Fe} cm^{-2} (reduced state).

Figure 3 demonstrates that r_{NH_3} increases significantly when H_2 is supplied to the cathode, thus going from "classic" to "mixed" configuration. The experimental results further show that the ammonia formation rate r_{NH_3} did not decrease but increased when the electrochemical ion supply was deliberately suppressed ("blocked" configuration).

These observations suggest that protons conducted through the electrolyte may negatively impact at the cathode's surface. Since the H_2 concentration is similar in both configurations ("mixed" and "blocked"), with only a slight increase in the "mixed" configuration due to the HER, molecular H_2 does not appear to negatively influence the process. But protons flux may lead to occupied active catalyst sites, thereby hindering the adsorption and dissociation of N_2 and reducing the selectivity toward NH_3 formation, as also reported by other authors.[9,19] Furthermore, the results indicate that EPOC, caused by the supply of ionic species in an electric field, either does not contribute significantly to ammonia synthesis or does not adequately describe the underlying process. The isolated effect of the electric field on ammonia formation have been shown in fixed-bed experiments, with observed significant rate enhancements pointing to enhanced N_2 activation steps under field application.[27] This could be explained by the applied voltage, which shifts the Fermi level of a thin metal catalyst layer, thereby altering the partial density of states and enhancing the availability of active electronic states for catalytic reactions.[28] Specifically, a negative field induces electron transfer into the anti-bonding π^* orbitals of adsorbed N_2 molecules, which weakens the N≡N bond and facilitates the formation of Fe–N intermediates, a key step in nitrogen activation.[29]

The highest r_{NH_3} were obtained at −1.4 V for each gas configuration, with 1.42×10^{-10} mol cm^{-2} s^{-1} ($j = 0.116$ A cm^{-2}), 3.23×10^{-9} mol cm^{-2} s^{-1} ($j = 0.073$ A cm^{-2}) and 4.32×10^{-9} mol cm^{-2} s^{-1} ($j = 0.269$ A cm^{-2}) for the "classic," "mixed" and "blocked" configurations, respectively.

The green dashed line represents the thermodynamic equilibrium at 500 °C for a 1:1 H_2:N_2 mixture at the cathode without the supply of current and is technically only applicable for the "blocked" configuration where no additional H_2 is added by proton pumping. As can be seen from the diagram, configuration "blocked" approaches this equilibrium asymptotically and thus appears to be limited. In contrast, the "mixed" configuration does not yet appear to be thermodynamically limited, but since the corresponding equilibrium line would increase with voltage due to H_2 production at the cathode by HER, limitation may also be shifted to slightly higher formation rates.

In the "classic" configuration, NH_3 formation is the lowest. As expected, the reduced H_2 concentrations in the cathode gas phase in this configuration negatively impacts the system, as the low partial pressure of H_2 restricts NH_3 formation. The H_2 concentration in the gas coming from the cathode was quantified by mass spectrometry (MS) under both OCV and an applied potential of −1.4 V, yielding values of 1.08% and 2.75%, respectively. These concentrations form the basis for the thermodynamic equilibria presented at the corresponding voltages in Fig. 3. As indicated by the course of the NH_3 production rates operating in the "classic" configuration, NH_3 synthesis appears to be thermodynamically constrained at high absolute voltages, making a higher H_2 partial pressure at the cathode essential.

Figure 4 provides in (a) the electrochemical Faraday efficiency for NH_3, FE_{NH_3}, the corresponding current density j (b) and the enhancement factors ρ (c) as a function of the cell voltage for the three gas configurations at 500 °C.

FE_{NH_3} of gas configuration "classic" remains below 0.05% across all applied voltages, while the rate enhancement factor ρ, reaches its maximum value of approximately 8 at −1 V.

For gas configuration "mixed," FE_{NH_3} peaks at 1.2%, and ρ attains a value of 21 at −1.4 V, representing one of the highest enhancement factors reported in the literature (compare Table I). Both FE_{NH_3} and ρ for the "mixed" configuration do not exhibit asymptotic behavior at the highest absolute voltages, in contrast to the other two gas configurations.

Gas configuration "blocked" demonstrates the highest rate enhancement value, appearing to plateau below $\rho = 24$. FE_{NH_3} for configuration "blocked" shows a strong initial increase, followed by a sharp decline at higher absolute voltages. This decline can be attributed to the very high current densities required to achieve higher absolute voltages in this configuration. As shown in Fig. 4b, j at −0.8 V is 0.054 A cm^{-2} and 0.016 A cm^{-2} for the "mixed" and "blocked" configurations, respectively. At −1.4 V, a higher j value of 0.269 A cm^{-2} is observed in the "blocked" configuration, whereas a lower value of 0.073 A cm^{-2} is found in the 'mixed' configuration. Moderate polarization in "blocked" configuration results in significantly enhanced efficiency for NH_3 synthesis. This improvement may be due to the elimination of H_2 supply to the anode, which suppresses side reactions such as HER at the cathode ($2\,OH_O^{\bullet} + 2e^- \rightarrow H_2$). In this way, possible H_2 poisoning on the catalyst surface is reduced. These results are consistent with the findings of Li et al., who demonstrated through isotope labeling experiments that electrochemical NH_3 formation is predominantly governed by surface reactions with H_2 from the gas phase, while protons supplied by the electrolyte contribute only marginally.[30]

It is important to note that the "blocked" configuration becomes unstable, exhibiting significant voltage fluctuations and shifts when the cell is operated for several hours at voltages below −0.8 V (See Fig. S4). Repeating the experiment for the "blocked" configuration with the same cell was hardly feasible due to the ever-increasing current densities required to reach a certain cell voltage. This suggests that irreversible changes occur within the cell during this gas configuration that are not reversible, even if H_2 is added after prolonged operation.

This behavior observed in the "blocked" configuration can be attributed to the imposed cell voltage in the absence of effective ionic transport. When a current is externally applied (e.g. under galvanostatic conditions) but proton conduction through the electrolyte is prevented, the current must be sustained by alternative mechanisms. These mechanisms may include electronic leakage currents through the electrolyte, or capacitive contributions resulting from the charging and discharging of electric double layers at the electrode–electrolyte interfaces.

Moreover, reduction of Ce^{4+} to Ce^{3+} within the BCZY721 electrolyte is possible under reducing conditions and elevated potentials. Mortalò et al. demonstrated through temperature-programmed reduction (TPR) and thermogravimetric analysis (TGA)

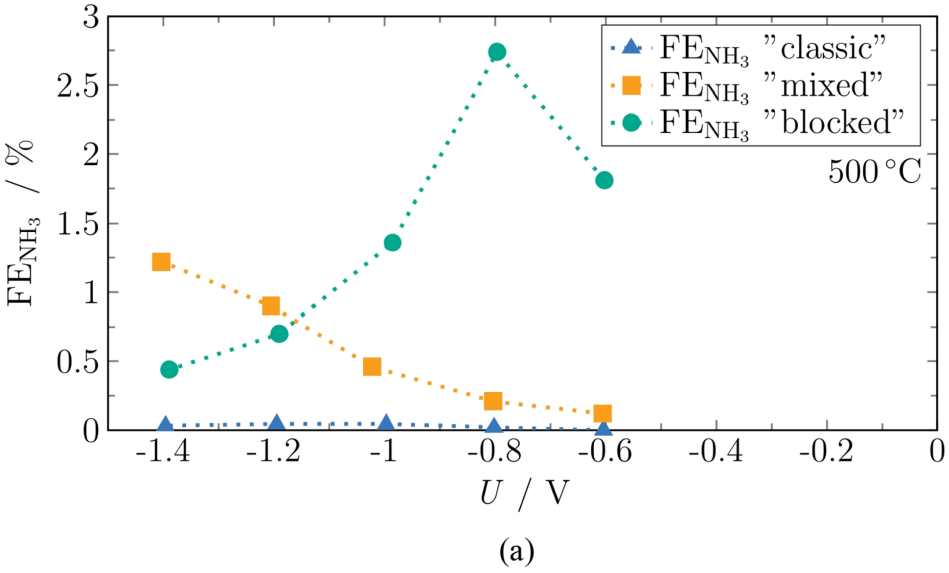

(a)

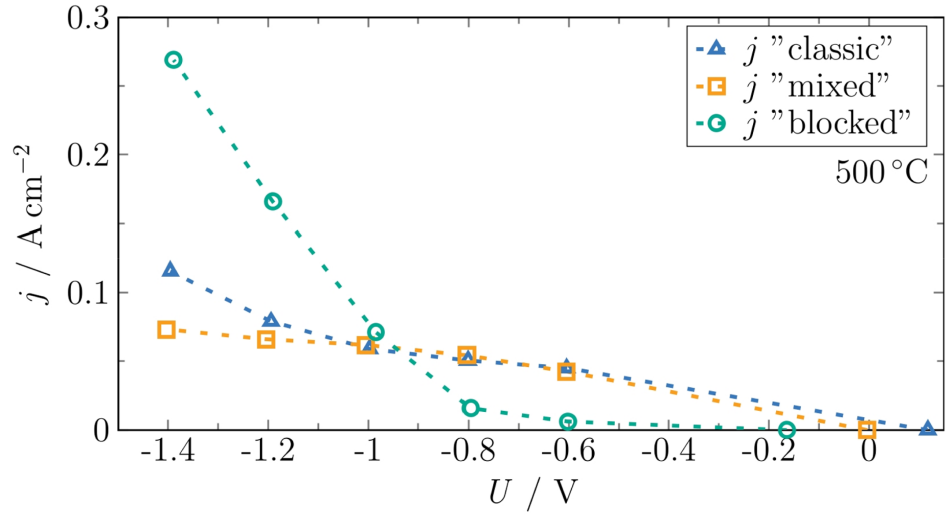

(b)

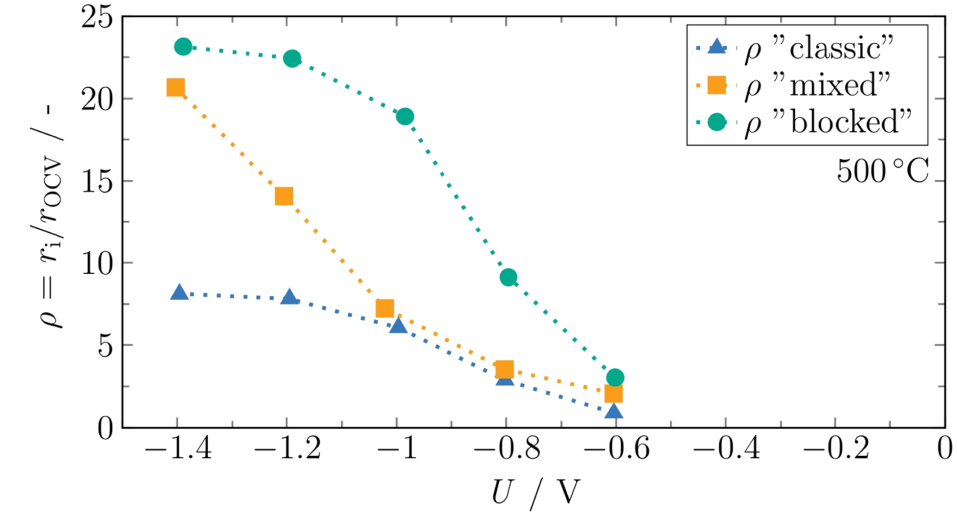

(c)

Figure 4. (a) Electrochemical Faraday efficiency FE_{NH_3}, (b) current density j and in (c) the enhancement factors ρ for the three gas configurations in Fig. 3.

that $BaCe_{0.65}Zr_{0.20}Y_{0.15}O_{3-\delta}$ undergoes partial reduction of Ce^{4+} to Ce^{3+} under reducing atmospheres, with a prominent peak observed around 500 °C.[31] This temperature of 500 °C corresponds to the temperature that was mainly used in our experiments, and Mortalò et al. also notes that structural changes were observed in the BCZY even without applying current.

With the reduction of Ce^{4+}, oxygen loss from the lattice occurs, leading to the formation of oxygen vacancies ($O_O^x \rightarrow 0.5O_2(g) + V_O^{\bullet\bullet} + 2e^-$).

Figure 5 shows the morphological changes in a cell exposed to the "blocked" configuration, in comparison to an unaltered electrolyte, which operated under continuous H_2 supply to the anode. The SEM images reveal distinct alterations in the electrolyte after several hours of operation under the "blocked" configuration. Notably, small cracks (mean: 232 nm, range: 129 nm to 335 nm) have developed along the grain boundaries, indicating localized mechanical or chemical strain. This pronounced morphological impact demonstrates that, despite the comparable electrochemical results, the "blocked" configuration is not suitable for electrochemical NH_3 synthesis.

Effect of volume flow.—Additionally, the effect of the cathode volume flow in configuration "mixed" was investigated at a fixed H_2:N_2 ratio of 1:1. During testing, a constant H_2 flow rate of 6 NL h^{-1} was maintained at the anode, while the cathode volume flow was incrementally increased from 8 NL h^{-1} to 20 NL h^{-1}. For each flow rate NH_3 quantification was conducted at OCV and an applied voltage of −1 V for a constant temperature of 500 °C and at 600 °C. The corresponding r_{NH_3} are presented in Fig. 6. The associated thermodynamic equilibrium at the respective temperature for a ratio of H_2:N_2 of 1:1 is also included.

Figure 6 illustrates the dependency of r_{NH_3} on volume flow for the same cell type utilizing iron as a catalyst, with a loading of 2.7 mg_{Fe} cm^{-2} each. The increase in NH_3 formation for a gas supply change from 8 NL h^{-1} to 20 NL h^{-1} at −1 V is a factor of 3.1 at both 500 °C and 600 °C. At OCV, the increase is a factor of 3.0 at 600 °C and 3.4 at 500 °C. Both the NH_3 formation rates at OCV and at −1 V exhibit a more-than-proportional increase with increasing gas flow rates. This behaviour may result from mass transport limitations at lower flowrates and/or the thermal decomposition of NH_3 at 500 °C and especially 600 °C, where longer gas residence times can enhance reverse reaction pathways. This trend was similarly observed in packed-bed reaction experiments indicating that the volume flow has a significant impact on the formation rates of ammonia.[32,33]

Moreover, the rate enhancement factor ρ remains stable within the range of 8 NL h^{-1} to 20 NL h^{-1} for each temperature. Here, ρ is significantly higher during operation at 500 °C compared to 600 °C. This may be attributed to the fact that NH_3 formation at 600 °C appears to be thermodynamically limited, as also seen by the occurrence of a plateau with further decreases in cell voltage. Even further reducing the voltage from −1 V to −1.2 V does not change r_{NH_3} in a noticeable way. In contrast, at 500 °C, ρ is significantly higher, but NH_3 formation is significantly lower than the thermodynamic equilibrium. However, as the voltage decreases further, r_{NH_3} asymptotically approaches the thermodynamic equilibrium, as illustrated in Fig. 3. It is important to note that the thermodynamic equilibrium is calculated for a fixed H_2:N_2 ratio of 1:1 without the supply of current and the apparent overperformance compared to the equilibrium at 600 °C can be caused by the slight excess of hydrogen at the cathode due to the proton flux.

Influence of electrolyte thickness.—The influence of electrolyte thickness on cell performance and r_{NH_3} was investigated using two cells with BCZY721 electrolytes of approximately 26 μm (thick) and 13 μm (thin), respectively. The catalyst loading at the working electrode was maintained nearly constant, at 2.7 mg_{Fe} cm^{-2} for the

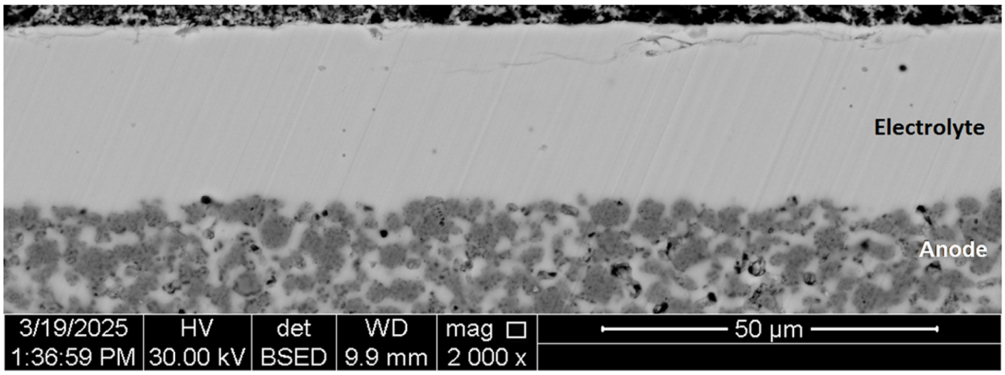

(a)

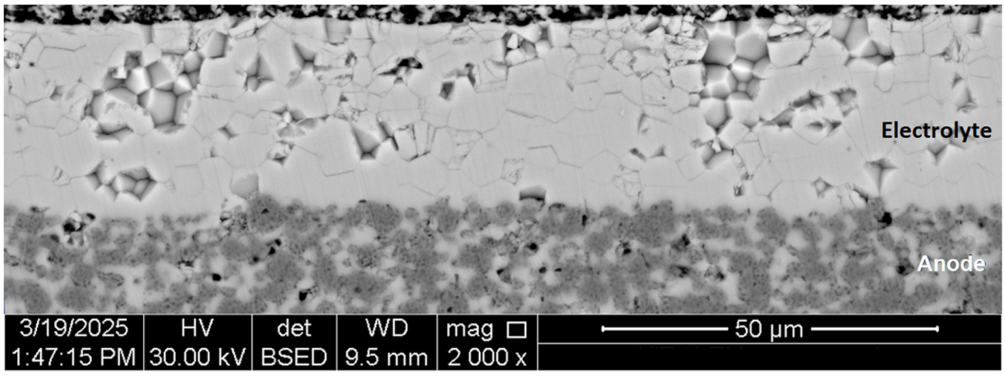

(b)

Figure 5. Cross-sectional SEM images of a PCC after reduction and two weeks of operation. The bottom layer is the Ni-BCZY811 anode, the middle layer is the BCZY721 electrolyte, and the top layer is the iron-based electrode. The light and dark phases correspond to BCZY and Ni, respectively. Cell in (b) was additionally operated in the "blocked" configuration.

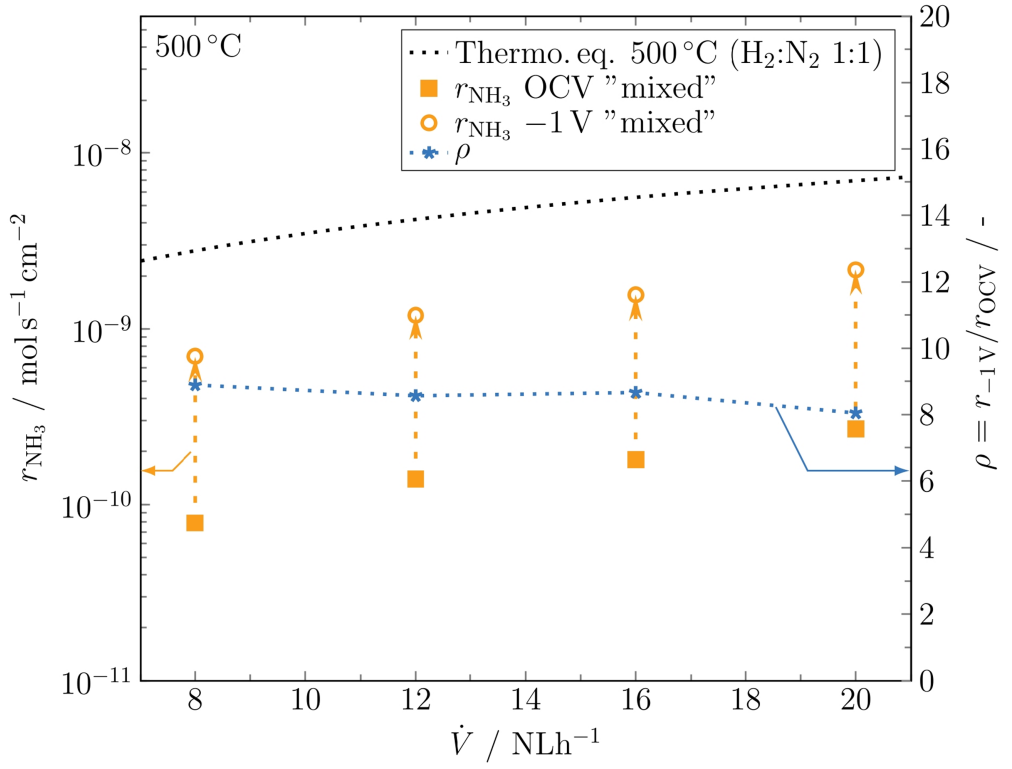

(a)

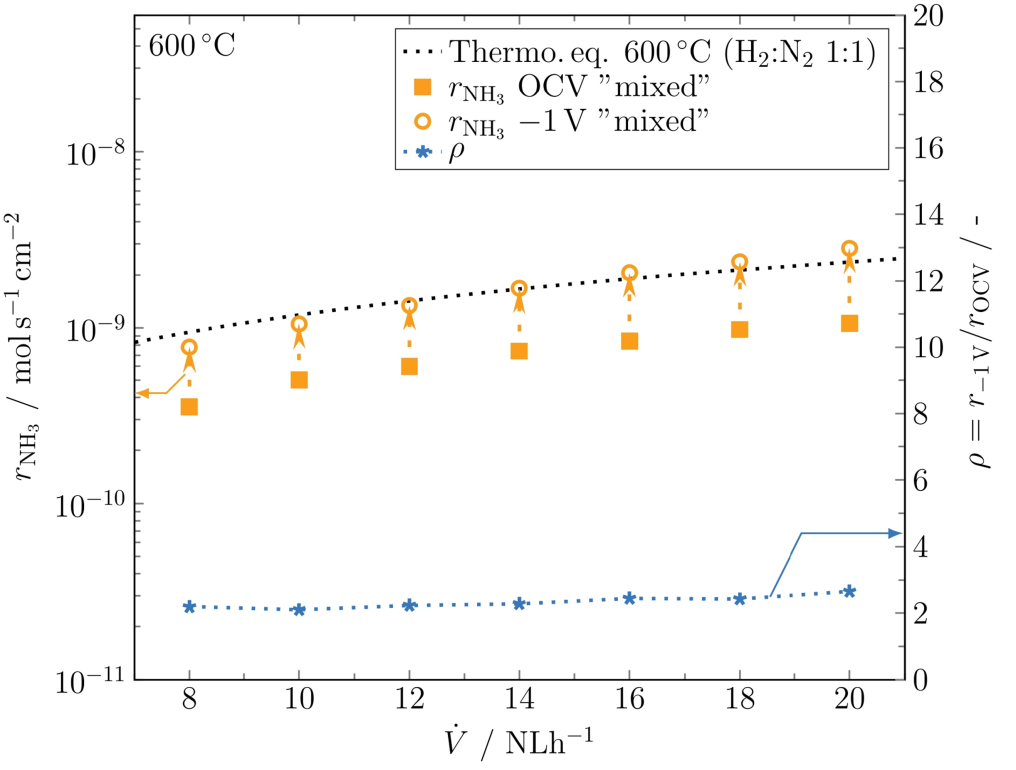

(b)

Figure 6. NH_3 formation r_{NH_3} as a function of volume flow to the cathode for the "mixed" configuration from Table III, conducted at 500 °C (a) and 600 °C (b). NH_3 downstream quantification conducted at OCV and at a cell voltage of −1 V. The thermodynamic equilibrium (black, dotted) is calculated for an active area of 12.57 cm^2 and a H_2:N_2 of 1:1 at OCV. The enhancement factor ρ for the respective volume flow is displayed in blue stars.

thick electrolyte and 2.5 mg_{Fe} cm^{-2} for the thin electrolyte. Both cells were operated at 500 °C in the "mixed" configuration.

Figure 7a illustrates the NH_3 formation of two cells with different electrolyte thicknesses across a potential range from OCV to −1.4 V. The formation rates are nearly identical at low absolute voltages and below −1 V, with deviations observed at intermediate voltages. Notably, the thinner electrolyte exhibits a higher r_{NH_3} in this range. Figure 7b presents the corresponding current density j and FE_{NH_3} for both cells. The results obtained demonstrate that a thinner electrolyte results in higher current densities at the same applied voltage compared to a thicker electrolyte, which can be explained by the reduction in ohmic resistance. This indicates that NH_3 formation is more strongly influenced by the applied voltage than by the current density, as also reported by Li et al.[12] Furthermore, the results imply that the current density has no significant impact on overall NH_3 formation. However, due to the lower FE_{NH_3} observed for the thinner electrolyte, and the corresponding higher current densities, thicker electrolytes may offer advantages in terms of overall efficiency for electrochemical NH_3 synthesis.

The differences between the thick and thin electrolyte are further investigated using electrochemical impedance spectroscopy, displayed as Nyquist plots in Fig. 8, measured at 500 °C and at OCV.

For an easier comparison between the diagrams of the thick and thin electrolyte, the respective contributions fitted by an equivalent circuit (Fig. 9) are listed in Table IV. The model contains three key components: an inductance L, which accounts for inductive effects caused by wiring or connections, and an ohmic resistance R_0, representing the intrinsic resistance of the electrolyte or other materials in the system. Additionally, the model includes two resistor-constant phase element (R-CPE) components that describe the non-ideal capacitive behavior of the electric double layer at the electrode/electrolyte interface and charge transfer processes within the system. The constant phase element (CPE) accounts for deviations from ideal capacitor behavior due to surface roughness, inhomogeneities, or other factors. Furthermore, mass transfer limitations, such as the diffusion of reactants and products, can also be modeled using R-CPE's. The exponent α in the CPE characterizes its deviation from ideal capacitive behavior. For $\alpha < 1$, the CPE represents a non-ideal capacitive response, often associated with surface inhomogeneities, diffusion effects, or distributed time constants. The overall fitting error using the proposed equivalent circuit for the impedance spectra remained less than or equal to about 0.5% for both cell thicknesses. In addition, the phase angle error was below 0.02°, indicating a high degree of conformity in fitting the impedance data.

As shown in the Nyquist plots in Fig. 8, the cell with the thinner electrolyte exhibits significantly lower total impedance, with a reduction in both the ohmic and polarization resistance. The observed approximately twofold reduction in ohmic resistance R_0

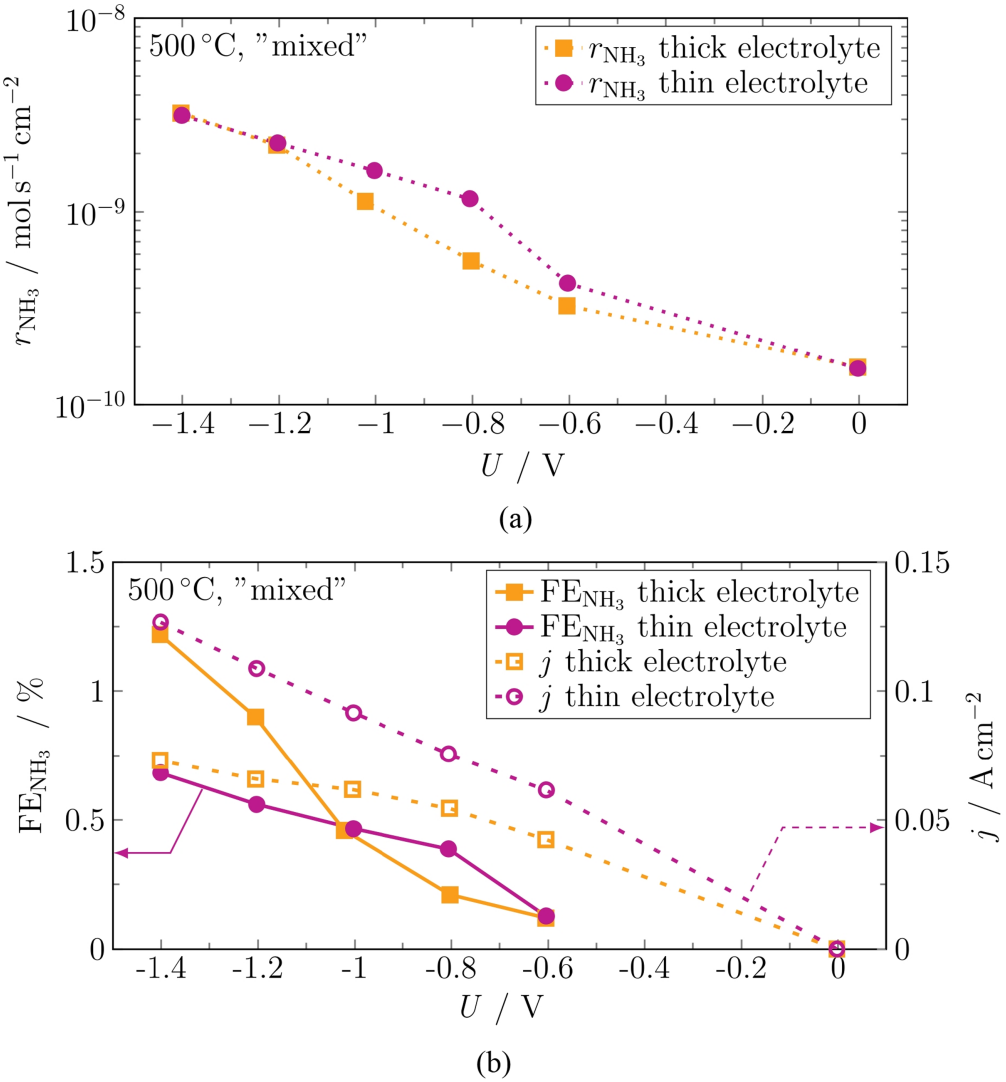

Figure 7. (a) NH_3 formation r_{NH_3} for a thick and thin electrolyte at 500 °C in the "mixed" configuration with a constant volume flow of 12 NL h^{-1} to the cathode. (b) Electrochemical Faraday efficiency FE_{NH_3} in % and the respective current density for both cell types.

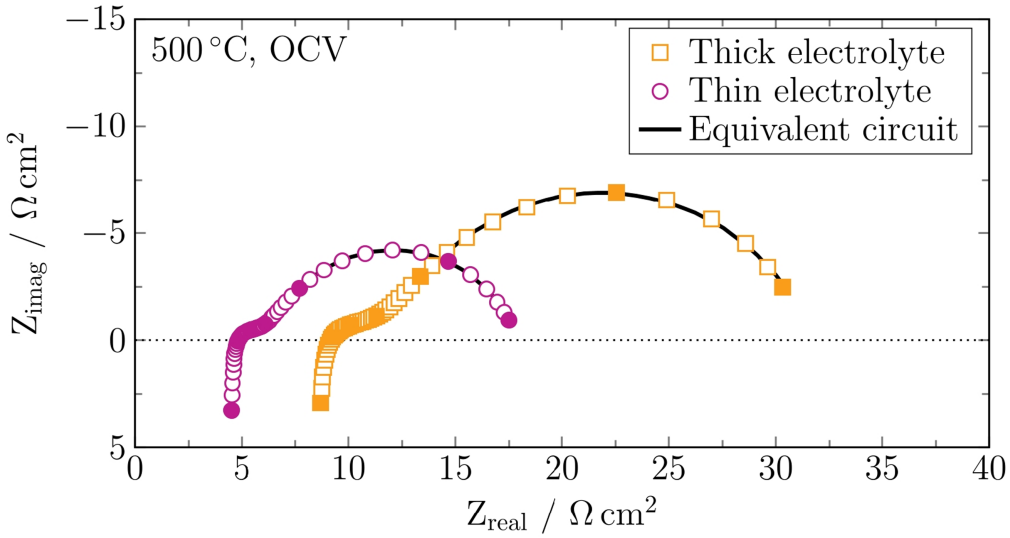

Figure 8. Comparison of the Nyquist plots of the tested cells with thick (orange squares) and thin electrolyte (purple circles), color-filled marks highlight the decades for the frequency range 100 mHz to 100 kHz. The dashed lines show the modeled spectra with the equivalent circuit in Fig. 9.

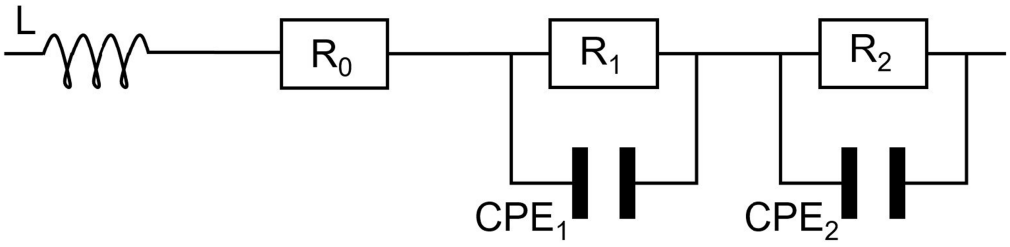

Figure 9. Equivalent circuit model used to fit the impedance spectra.

Table IV. Electrochemical comparison between the thick and thin cell fitted by the equivalent circuit model presented in Fig. 9.

Cell:	Thick	Thin
L [H cm^{-2}]	5.10×10^{-6}	5.38×10^{-6}
R_0 [Ω cm^2]	8.12	4.29
R_1 [Ω cm^2]	17.98	11.25
R_2 [Ω cm^2]	5.91	2.40
CPE_1 [F cm^{-2}]	12.65×10^{-3}	11.85×10^{-3}
α_1 [−]	0.794	0.800
CPE_2 [F cm^{-2}]	20.84×10^{-3}	11.93×10^{-3}
α_2 [−]	0.312	0.427
Overall fitting error [%]	0.503	0.385
Mean phase angle error [°]	0.0135	0.0173

is consistent with the expected difference based on electrolyte thickness and is attributed to the shorter ionic conduction path and reduced ohmic losses within the thinner electrolyte layer. The R_1 resistance associated with the low-frequency arc can be attributed to transport processes within both the electrode and the electrolyte, whereas the middle-frequency arc associated with R_2 can reflect various fast interfacial processes, including surface adsorption and dissociation, charge transfer at the electrode/electrolyte interface, and possible contributions from ionic conduction within the electrode or interfacial capacitance. An increase in the resistance of the low-frequency arc with increasing electrolyte thickness attributable to transport processes within the electrolyte is evident and has also been observed in other studies investigating varying electrolyte thicknesses.[34]

The corresponding Bode plots (See Fig. S5) further support this observation, with the thinner electrolyte consistently showing a lower impedance across the entire frequency range. The high-frequency asymptote shows the ohmic electrolyte resistance, and the low-frequency asymptote shows the sum of the polarization impedance and electrolyte resistance. When the phase angle is plotted as a function of frequency, the impedance of the cell with the thinner electrolyte results in an increased phase shift and a shift of the relaxation frequency toward higher values, both of which are indicative of faster dynamic processes.

Conclusions

The results of the experimental study indicate that NH_3 production is primarily influenced by the applied cell voltage and not by the current density. A comparison of different gas configurations at the cell reveals enhanced NH_3 formation in a configuration in which proton transport through the electrolyte is inhibited, even if this configuration is not stable over time, resulting in increased current/power requirements and a damaged electrolyte. These results also indicate that EPOC, as defined by the supply of ionic species and an electric field, either does not contribute significantly to ammonia synthesis or does not adequately describe electrochemical ammonia synthesis. They also indicate that the proton transport through the electrolyte plays a minor or even no role in the electrochemical synthesis of NH_3 on an iron-based electrode on a PCC. A possible reason is surface H_2 poisoning on the catalyst, which inhibits nitrogen adsorption and consequently catalytic activity. The experimental findings also highlight the significant impact of the thermodynamic equilibrium on the achievable NH_3 yield. Lower operating temperatures and higher volumetric flow rates per unit cell area were found to be beneficial. In addition, lower temperatures were associated with an increase in the rate enhancement factor, reaching

values as high as 24, which is high compared to those reported in the literature.

From an operational perspective, it was found that the "classic" gas configuration, where protons are pumped to the cathode, to which only N_2 is supplied, is thermodynamically constrained. This underscores the importance of co-feeding H_2 to the cathode to optimize reaction conditions and NH_3 production rates. By introducing H_2 to the cathode, the ammonia synthesis rate increased from 1.42×10^{-10} mol cm^{-2} s^{-1} ("classic" configuration) to 3.23×10^{-9} mol cm^{-2} s^{-1} ("mixed" configuration) at a cell voltage of -1.4 V and 500 °C. When proton conduction was suppressed under the same conditions, r_{NH_3} increased to 4.32×10^{-9} mol cm^{-2} s^{-1} ("blocked" configuration). While the present r_{NH_3} are highly encouraging, significant advances are still required to achieve commercially viable ammonia production levels.

The experimental investigations were carried out using a PCC with an iron-based electrode with an active area of 12.57 cm^2, which represents the largest electrode area reported to date for electrochemical NH_3 synthesis.

Acknowledgments

We acknowledge the support by omegadot software and consulting GmbH for providing the software tool DETCHEM. This project was funded by the Deutsche Forschungsgemeinschaft (DFG, German Research Foundation) − 460038541 under the NSF-DFG Echem initiative (DE 659/14-1).

ORCID

Philipp Blanck https://orcid.org/0009-0000-3683-2704
Etienne P. Martin https://orcid.org/0009-0008-8814-0898
Daniel Schmider https://orcid.org/0000-0003-2158-6007
Robert J. Kee https://orcid.org/0000-0003-3930-4784
Julian Dailly https://orcid.org/0000-0002-4853-3661
Olaf Deutschmann https://orcid.org/0000-0001-9211-7529

References

1. World Economic Forum, (2022), https://weforum.org/reports/the-net-zero-industry-tracker/in-full/ammonia-industry.
2. IEA, (2021), https://iea.org/reports/ammonia-technology-roadmap.
3. M. Liang, J. Kim, X. Xu, H. Sun, Y. Song, S. Jeon, T. H. Shin, Z. Shao, and W. Jung, *Energy Environ. Sci.*, **18**, 3526 (2025).
4. H. M. Vieri, M.-C. Kim, A. Badakhsh, and S. H. Choi, *Energies*, **17**, 441 (2024).
5. Q. Hu, C. Tian, D. Bao, H. Zhong, and X. Zhang, *Energy*, **4**, 100144 (2024).
6. M. Stoukides and C. G. Vayenas, *J. Catal.*, **70**, 137 (1981).
7. C. G. Vayenas, P. Vernoux, P. Vernoux, and C. G. Vayenas, *Recent Advances in Electrochemical Promotion of Catalysis* (Springer International Publishing, Cham) 61, 3 (2023).
8. S. Bebelis, *Recent Advances in Electrochemical Promotion of Catalysis*, ed. P. Vernoux and C. G. Vayenas (Springer International Publishing, Cham) 61, 21 (2023).
9. E. Vasileiou, V. Kyriakou, I. Garagounis, A. Vourros, A. Manerbino, W. G. Coors, and M. Stoukides, *Top. Catal.*, **58**, 1193 (2015).
10. I. Garagounis, V. Kyriakou, and M. Stoukides, *Solid State Ion.*, **231**, 58 (2013).
11. A. Vourros, I. Garagounis, and M. Stoukides, *Recent Advances in Electrochemical Promotion of Catalysis*, ed. P. Vernoux and C. G. Vayenas (Springer International Publishing, Cham) 61, 303 (2023).
12. C.-I. Li, H. Matsuo, and J. Otomo, *Sustain. Energy Fuels*, **5**, 188 (2021).
13. E. Vasileiou, V. Kyriakou, I. Garagounis, A. Vourros, and M. Stoukides, *Solid State Ion.*, **275**, 110 (2015).
14. E. Vasileiou, V. Kyriakou, I. Garagounis, A. Vourros, A. Manerbino, W. G. Coors, and M. STOUKIDES, *Solid State Ion.*, **288**, 357 (2016).
15. F. Kosaka, T. Nakamura, A. Oikawa, and J. Otomo, *ACS Sustain. Chem. Eng.*, **5**, 10439 (2017).
16. M. Okazaki and J. Otomo, *ACS Omega*, **8**, 40299 (2023).
17. I. Garagounis, A. Vourros, D. Stoukides, D. Dasopoulos, and M. Stoukides, *Membranes*, **9**, 112 (2019).
18. I. A. Amar, R. Lan, C. T. G. Petit, and S. Tao, *J. Solid State Electrochem.*, **15**, 1845 (2011).
19. I. Garagounis, V. Kyriakou, A. Skodra, E. Vasileiou, and M. Stoukides, *Front. Energy Res.*, **2**, 1–10 (2014).
20. W. B. Wang, X. B. Cao, W. J. Gao, F. Zhang, H. T. Wang, and G. L. Ma, *J. Membr. Sci.*, **360**, 397 (2010).
21. M. Ouzounidou, A. Skodra, C. Kokkofitis, and M. Stoukides, *Solid State Ion.*, **178**, 153 (2007).
22. M. Okazaki and J. Otomo, *Ind. Eng. Chem. Res.*, **63**, 17413 (2024).
23. P. Blanck, D. Schmider, R. J. Kee, J. Dailly, and O. Deutschmann, *Ceram. Int.*, S0272884225022825 (2025).
24. O. Deutschmann et al., (2022), www.detchem.com.
25. I. J. McPherson, T. Sudmeier, J. Fellowes, and S. C. E. Tsang, *Dalton Trans.*, **48**, 1562 (2019).
26. A. Moranti, J. Dailly, M. Santarelli, and F. Smeacetto, *Energy Convers. Manag.*, **321**, 119082 (2024).
27. R. Manabe, H. Nakatsubo, A. Gondo, K. Murakami, S. Ogo, H. Tsuneki, M. Ikeda, A. Ishikawa, H. Nakai, and Y. Sekine, *Chem. Sci.*, **8**, 5434 (2017).
28. M. Shetty et al., *ACS Catal.*, **10**, 12666 (2020).
29. L. Rincón, F. Ruette, and A. Hernández, *J. Mol. Struct. THEOCHEM*, **254**, 395 (1992).
30. C.-I. Li, H. Matsuo, and J. Otomo, *RSC Adv.*, **11**, 17891 (2021).
31. C. Mortalò, M. Boaro, E. Rebollo, V. Zin, E. Aneggi, M. Fabrizio, and A. Trovarelli, *ACS Appl. Energy Mater.*, **3**, 9877 (2020).
32. C. Karakaya, J. Huang, C. Cadigan, A. Welch, J. Kintner, J. Beach, H. Zhu, R. O'Hayre, and R. J. Kee, *Chem. Eng. Sci.*, **247**, 116902 (2022).
33. Z. Zhang, C. Karakaya, R. J. Kee, J. D. Way, and C. A. Wolden, *ACS Sustain. Chem. Eng.*, **7**, 18038 (2019).
34. J. Melnik, A. R. Sanger, A. Tsyganok, J. L. Luo, and K. T. Chuang, *J. Power Sources*, **185**, 1101 (2008).